






Effect of Welding Speed on Microstructure and Anisotropic Properties of Wire-Arc Additive-Manufactured Ti-6Al-4V alloy

Guo Xian¹  · Jieun Yu¹  · Muralimohan Cheepu²  · Sang Myung Cho²  · Namhyun Kang¹ 

Received: 25 March 2022 / Accepted: 17 May 2022 / Published online: 10 June 2022
© The Indian Institute of Metals - IIM 2022

Abstract As a significant parameter required for welding, welding speed can be used to control the grain structure during the wire-arc additive manufacture of Ti64 alloy. Herein, the prior- β grain morphology and anisotropic tensile strength were examined to investigate the impact of welding speed after hammer peening treatment. Meanwhile, SYS-WELD was applied to conduct a numerical analysis of the weld pool morphology and thermal history at different welding speeds. According to the experiment results, equiaxed prior- β grains developed in the faster welding speed specimen (F) and mixture prior- β grains (equiaxed and columnar) took shape in the middle and slow welding speed specimen (M and S), which was consistent with the anisotropic property as observed in the fast welding speed specimen with lower anisotropic tensile strength than others. Meanwhile, simulation results demonstrated that a faster welding speed led to a lower temperature gradient (G) and a higher solidification rate (R) resulted in a larger number of equiaxed grains compared to the slower welding speed specimen.

Keywords Welding speed · Grain structure · Thermal history · Anisotropic property · Ti-6Al-4V · WAAM

1 Introduction

Currently, Ti-6Al-4V has become one of the most commonly used materials for various engineering settings, such as

power plants and aircrafts, which is attributed to its superior mechanical properties and excellent performance in corrosion resistance. Different from the conventional methods of production, wire + arc additive manufacturing (WAAM) is a promising technology that demonstrates such advantages as high material efficiency, short lead time and low cost [1]. More specifically, the welding method can be divided into two categories: gas tungsten arc welding (GTAW) and gas metal arc welding (GMAW). Even though GMAW and GTAW can be applied during WAAM processes, GMAW-based WAAM is still disadvantaged by less stability and the generation of more weld fume and spatter [2, 3].

Even though WAAM is considered a better alternative economically, the downside of it is that the solidification grains are prone to epitaxial growth from the adjacent melted substrate, thus leading to the development of columnar grains. Along the build direction, the undesirable columnar structure in WAAM is produced in Ti64, thus enhancing anisotropic tensile properties. Currently, some research has been conducted on the hammer peening effect on the transformation of grain structure from columnar to equiaxed [4]. However, in addition to hammer peening, welding speed is another influencing factor worth considering, which produces a different morphology of the weld pool [5–8]. When the microstructure solidifies from the weld metal, the shape of the weld pool exhibits a different temperature gradient (G) and solidification rate (R). During solidification process, there is a relationship between grain morphology, grain size, G and R. Previous studies have pointed out that equiaxed grain will quickly be produced from lower G and faster R. However, there is no more validation to explain its relationship.

This study is aimed to find an appropriate welding speed to cooperate with hammer peening treatments. Under these parameters, grain structure evolution and anisotropic

✉ Namhyun Kang
nhkang@pusan.ac.kr

¹ Department of Materials Science and Engineering, Pusan National University, Busan 46241, Republic of Korea

² Super-TIG Welding Co. Ltd, Busan 46722, Republic of Korea

property are deeply explained and analysed. Meanwhile, thermal history simulation has provided more reliable results to verify the relationship between grain morphology, G and R.

2 Experimental Procedure

WAAM specimens were produced with a GTAW using a C-type Ti64 consumable in order to match the wider arc morphology [9–11]. Table 1 lists the processing parameters used in this study, with three different welding speeds (F, M, S) taken into consideration. For constant welding parameters like current, voltage and feed rate, a faster welding speed reduces the width of deposition. After the welding of each layer, hammer peening treatment was carried out directly on the surface three times and surface temperature was usually measured to be about 200 °C before this treatment. With the interpass temperature maintained at a level below 80 °C, the collapse of the WAAM structure and the enlargement of grains were avoided. Argon gas (Ar, 99.99%) was also used as the trailing shield for the welding of Ti64 to prevent oxidation. The chemical composition of the filler metal (C-type) is shown in Table 2.

The Ti64 deposits were cut by half along the build and deposition directions. The transverse cross-section in the deposition direction was observed to grain structure. The prior-β grains were more easily identifiable in the longitudinal cross-section along the deposition direction. In order to reveal the grain boundaries, all of the samples were polished and etched using Kroll’s reagent. The prior-β grains morphology was examined by light optical microscopy (LOM). According to the ASTM E8/E8M-21 standard, the tensile specimens rescaled the proportion with a gauge length, width and thickness of 5 mm, 1.2 mm and 0.5 mm, respectively. Besides, a tensile test was performed on a minimum of three specimens under each welding condition at an initial strain rate of $0.5 \times 10^{-4} \text{ s}^{-1}$ (Shimadzu).

Table 1 Welding conditions of specimens F, M and S

C-type filler	Current (A)	Welding speed (mm/s)	Heat input (kJ/mm)
F	260	10	0.5
M	260	8	0.6
S	260	6	0.8

Table 2 Chemical composition of the filler metal (wt. %)

	Al	V	Fe	Cr	Mg	O	Ti
C-type	5.8	3.8	0.08	0.005	0.003	0.22	Bal

3 Numerical Model of Thermal Analysis

To simulate the process of Ti64 deposition, the finite-element method was applied to construct a thermal model with the assistance of SYSWELD (ESI). Figure 1 shows the models of the mesh constructed with 10 layers deposited for the thermal model of specimens, corresponding to the experimental morphology as observed. The height and width of the deposition block in models were identical to the measurements performed on the WAAM deposits for each layer. The mesh became finer when approaching the weld pool, which reduced the calculation time required for the model. The mesh geometry was established close to a hexahedron, and the size of the mesh was approximately 0.6 mm^3 . Table 3 lists the parameters used to construct the model. The governing differential equation for transient thermal analysis can be expressed as:

$$\rho c_p \frac{\partial T}{\partial t} = \frac{\partial}{\partial x} \left(k_x \frac{\partial T}{\partial x} \right) + \frac{\partial}{\partial y} \left(k_y \frac{\partial T}{\partial y} \right) + \frac{\partial}{\partial z} \left(k_z \frac{\partial T}{\partial z} \right) + \dot{q} \tag{1}$$

Figure 1 shows the power densities of the double-ellipsoid heat source during the WAAM process, denoted as $q_f(x, y, z)$ and $q_r(x, y, z)$, to describe the heat flux distributions in the front and rear quadrants, respectively. They are expressed as Eqs. (1 and 2) [12, 13]:

$$q_f(x, y, z) = \frac{6\sqrt{3}f_f Q}{a_f b c \pi \sqrt{\pi}} \cdot e^{-\frac{3x^2}{a_f^2}} \cdot e^{-\frac{3y^2}{b^2}} \cdot e^{-\frac{3z^2}{c^2}} \tag{2}$$

$$q_r(x, y, z) = \frac{6\sqrt{3}f_r Q}{a_r b c \pi \sqrt{\pi}} \cdot e^{-\frac{3x^2}{a_r^2}} \cdot e^{-\frac{3y^2}{b^2}} \cdot e^{-\frac{3z^2}{c^2}} \tag{3}$$

In this model, Q represents the effective heat power [W] and is expressed as $Q = \eta \cdot U \cdot I$, where η , U and I refer to the efficiency, welding voltage [V] and current [A], respectively. The variables f_f and f_r are the proportional coefficients at the front and rear ellipsoids of the heat source, respectively ($f_f + f_r = 2$). Meanwhile, a_f , a_r , b and c indicate the length/width/depth of the front/rear double ellipsoidal heat source parameters used to define the size and shape of the ellipses, respectively. Lastly, x , y and z denote the local coordinates of the reconstructed models. Boundary conditions are indicated as the red, green and blue arrows in the base metal surface, respectively. Three colours represent three directions, as fixed from the start time to the end time of welding. To simplify the finite-element thermal analysis, there were a number of assumptions made as follows:

- (1) The initial temperature of the model is set at 20 °C.

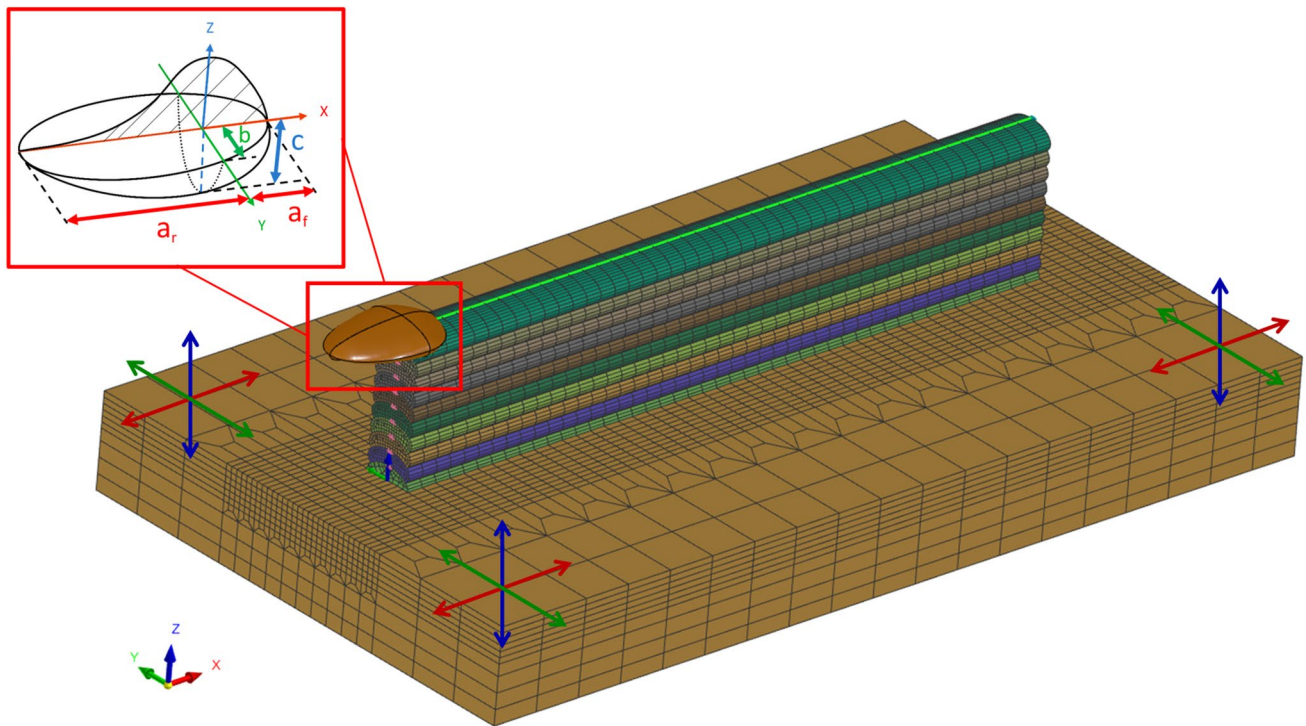


Fig. 1 Modelling for the finite-element mesh, boundary condition and the double-ellipsoidal (Goldak’s) heat source model

Table 3 Modelling parameters applied in SYSWELD

Model parameters	Conditions
Material (base and weld metals)	Ti-6Al-4 V
Density (kg/m ³)	4.5
Specific heat (J/kg·K)	7.2
Thermal conductivity (W/m·K)	560
Deposited layers (Z-direction)	10
Thickness of base metal (mm)	13
Interpass temperature (°C)	80
Ambient temperature (°C)	20
Element size (mm ³)	~0.6
Heat source parameter (af + ar)	15 mm
Heat source parameter (b)	5 mm
Heat source parameter (c)	2 mm
Arc type	TIG
Arc efficiency	60%

- (2) The fluid flow in the molten pool is negligible.
- (3) The heat transfer from the model to the environment can be defined at the surface of the model as the convective heat dissipation and radiation to the environment at 20 °C.

4 Results and Discussion

4.1 Grain Structure and Anisotropic Tensile Strength at Different Welding Speeds

There are two directions considered to observe the structures of prior-β grain. Figure 2a–c and e–f shows the cross-section of the specimen in the transverse and longitudinal directions, respectively. The transverse cross-section clearly reveals the geometry of the AM products as the height and width. The sample with a higher welding speed exhibits a smaller width of deposition (6.6 mm) compared to that with a lower welding speed. Meanwhile, equiaxed grains are observed in both cross-sections of specimen No. 1. However, when the welding speed decreases to the same level as specimen No. 2 or 3, the prior-β grain morphology is not an absolutely equiaxed one. Instead, it appears to be a mixture of grain structures (columnar and equiaxed grains) [14–16]. Even though all the samples undergo the same hammer peening treatment, the variation in welding speed still impacts the morphology of the grain structure. The amount of heat input into the deposition is larger during lower welding speeds compared to higher welding speeds. The heat exposure time is varied by changing welding speed and can enhance the grain growth [17–19]

Anisotropic tensile strength is clearly indicated in Fig. 3. At a higher welding speed, specimen No. 1 exhibits a weak

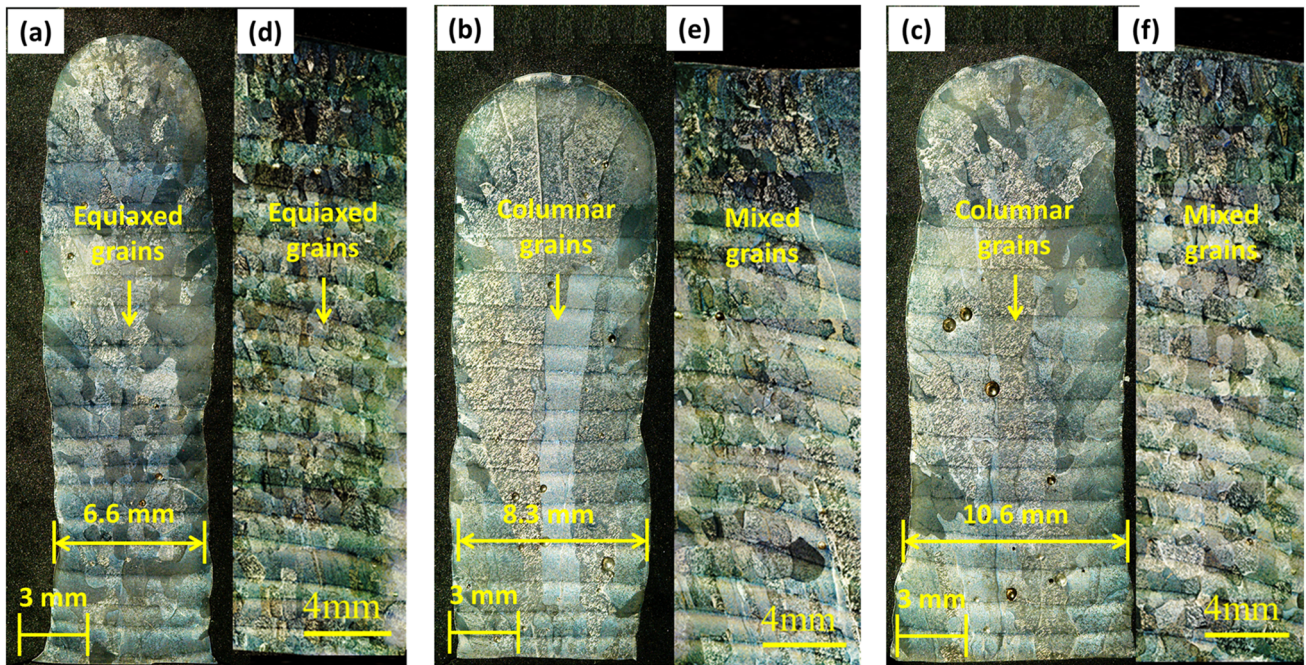


Fig. 2 Macro and solidification morphology observed for (a–c) transverse cross-sections and (d–f) longitudinal cross-sections of specimens F, M and S

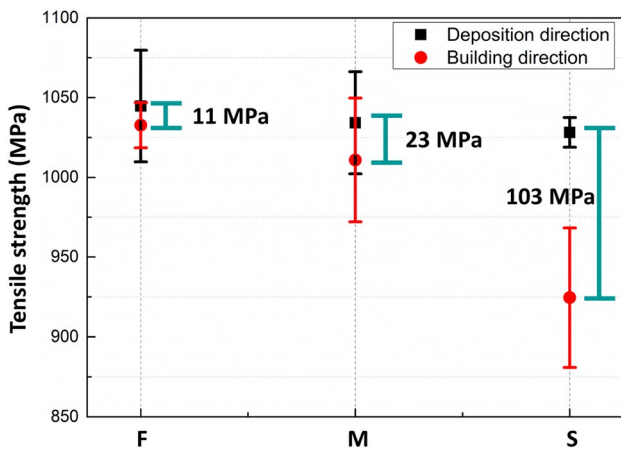


Fig. 3 Anisotropic tensile strength along the building and deposition directions of specimens F, M and S

anisotropic tensile strength of about 11 MPa. With the welding speed increasing, the anisotropy increases instantly to 23 MPa and 103 MPa, respectively. Previously, it was reported that grain morphology could make a difference to the anisotropic property [20, 21], which is consistent with the results of this study. Therefore, even though the specimens have undergone hammer peening treatment, a lower welding speed remains an optimal welding parameter needed to control the grain structure and reduce the anisotropic property.

4.2 Thermal History Simulation Results with Different Welding Speed

The weld pool geometry simulation results are presented in Fig. 4, while the overall view of the 5th deposition of WAAM products is shown in Fig. 4a, d and g. As the welding speed decreases, the width of deposition increases, as evidenced by the width of the weld pool geometry. The length of the weld pool in specimen Nos. 1 to 3 is about 29.8 mm, 26.7 mm and 25.4 mm, respectively. As for the simulation results, grey indicates that the temperature exceeds the melting temperature of 1660 °C, while the pink area is between the grey and red regions, with the temperature ranging from 1600 to 1660 °C, which is representative of the mushy zone. As a kind of solidification grain structure, prior- β grains tend to solidify in the mushy zone. During the solidification process, both G (temperature gradient) and R (solidification rate) play a vital role in the control of grain morphology and size. In general, the G and R in the weld pool vary constantly from the bottom to the rear due to the welding speed. In the centerline of the weld pool, the direction of growth is parallel to welding speed. Besides, the value of G reaches the minimum (G_{rear}) and R increases to the maximum (R_{rear}), which is the same as the welding speed as shown in Fig. 5. However, in the fusion line like the bottom of the weld pool, G_{btm} and R_{btm} are clearly opposite to the rear of the weld pool. Previously, high G_{btm} and low R_{btm} were mentioned

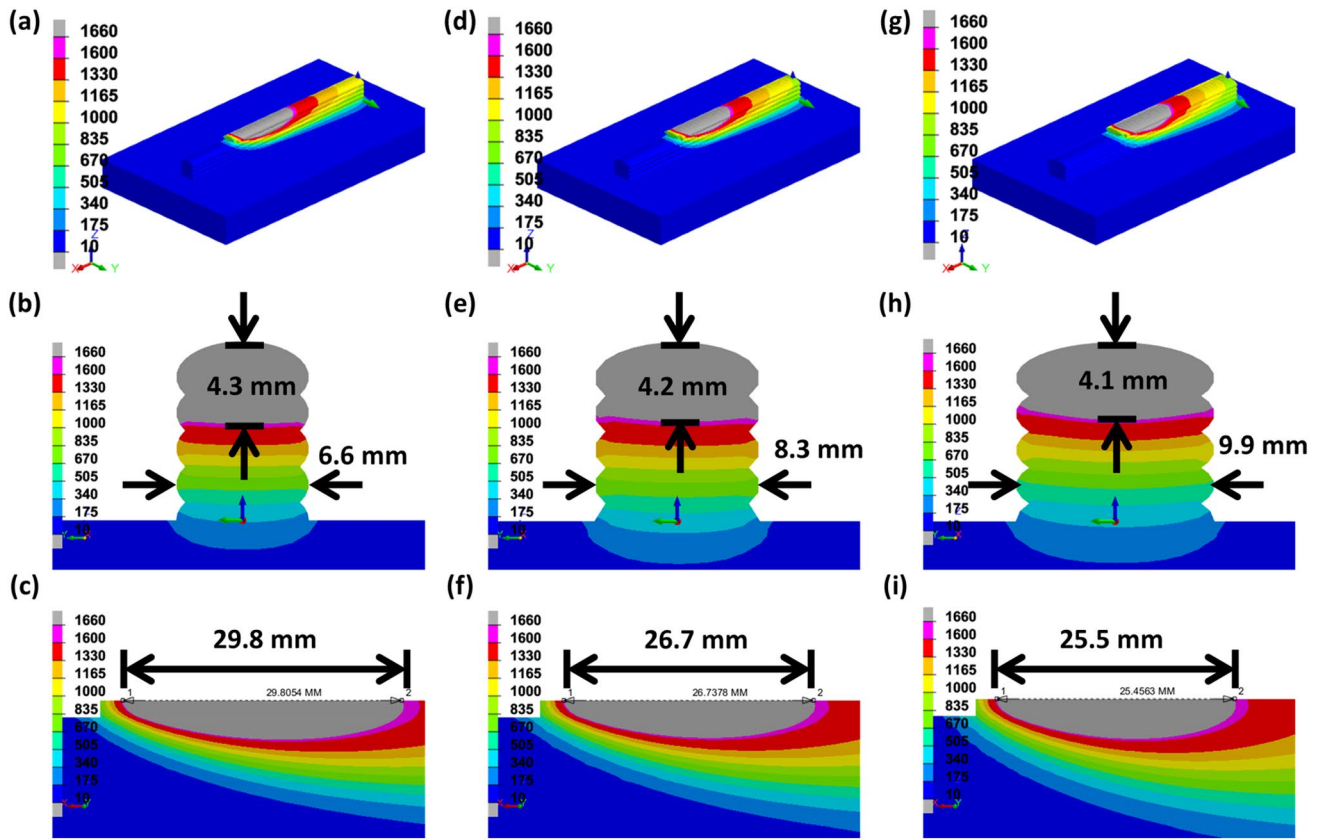


Fig. 4 Weld pool shape of 5th thermal cycles simulated in different perspectives for specimens F, M and S

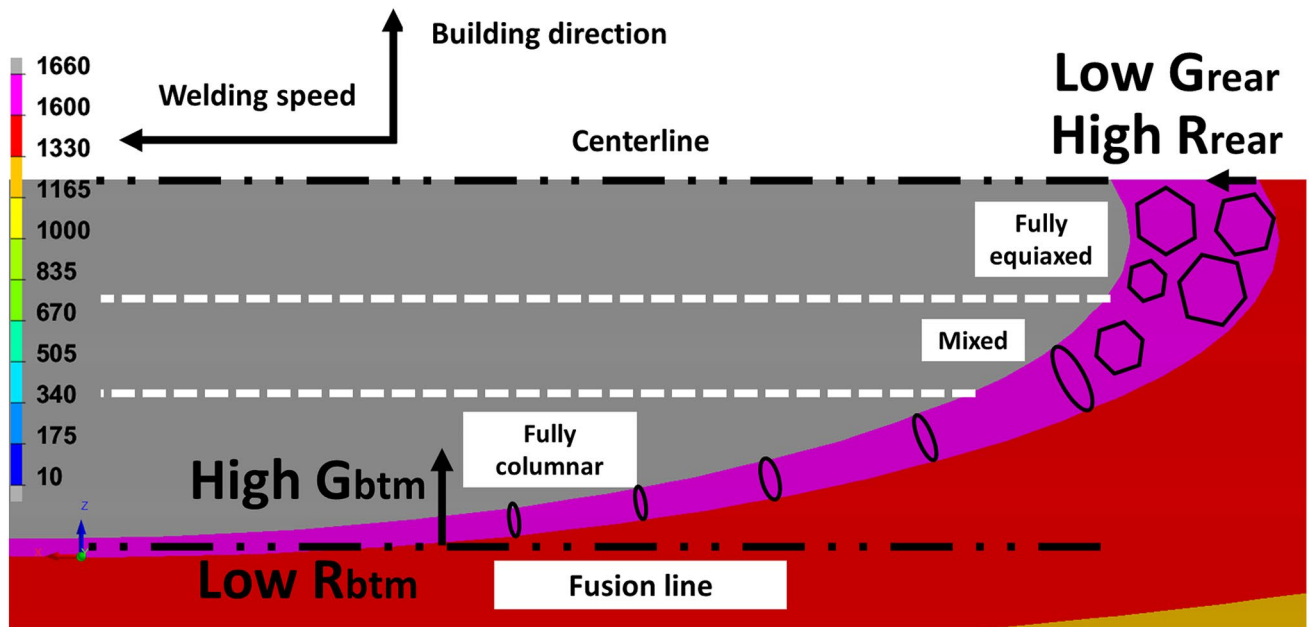


Fig. 5 Schematic illustration of the solidification grains evolution of the weld pool

as the result of narrow mushy zone, with the direction nearly perpendicular to the fusion line. The relationship between solidification rate (R) and welding speed (V) conforms to the following equation [15] (3):

$$R = V \cos \alpha \tag{4}$$

When α is 90 degrees, the R tends to the minimum value of approximately zero. The thermal history data in the weld pool bottom near the fusion line can be extracted from the node. Figure 6 shows the thermal histories of the specimen with three different welding speeds. Due to remelting, the 2nd thermal cycle was selected to analyse the morphology of solidification grains. The thermal history value of the simulation node in the fusion line is extracted and calculated, the cooling rates of which follow Eq. (4) [22]:

$$\text{Cooling rates} = G \times R \tag{5}$$

Within the solidification range (pink line) of 1600–1660 °C, the cooling rates have been calculated to be about 346, 315 and 257 °C/s in specimen Nos. 1, 2 and 3. According to the G (temperature gradient) value obtained from the simulation, the solidification rates (R) of these three specimens can be determined, as listed in Table 4. From the rear to the bottom of the weld pool, there are lower G and higher R shown in specimen No. 1 (fast welding

Table 4 G and R values calculated by SYSWELD in different specimens

Specimens	F	M	S
Welding speed (mm/s)	10	8	6
G_{rear} (°C/mm)	350	410	450
R_{rear} (mm/s)	10	8	6
Cooling rate $_{\text{btm}}$ (°C/s)	346	315	257
G_{btm} (°C/mm)	240	240	231
R_{btm} (mm/s)	1.4	1.3	1.1

speed) compared to other specimens, which explains the grain structure and anisotropic property.

5 Conclusion

Even though hammer peening treatment is effective in controlling the grain structure, welding speed is still not negligible. In this study, both experiments and numerical simulations were conducted to investigate the impact of welding speed on the grain structure and anisotropic properties of WAAM Ti-6Al-4V alloys.

- (1) A faster welding speed (F) exhibits far more equiaxed prior- β grains than other specimens (M and S) whether in the transverse or longitudinal cross-section. In addi-

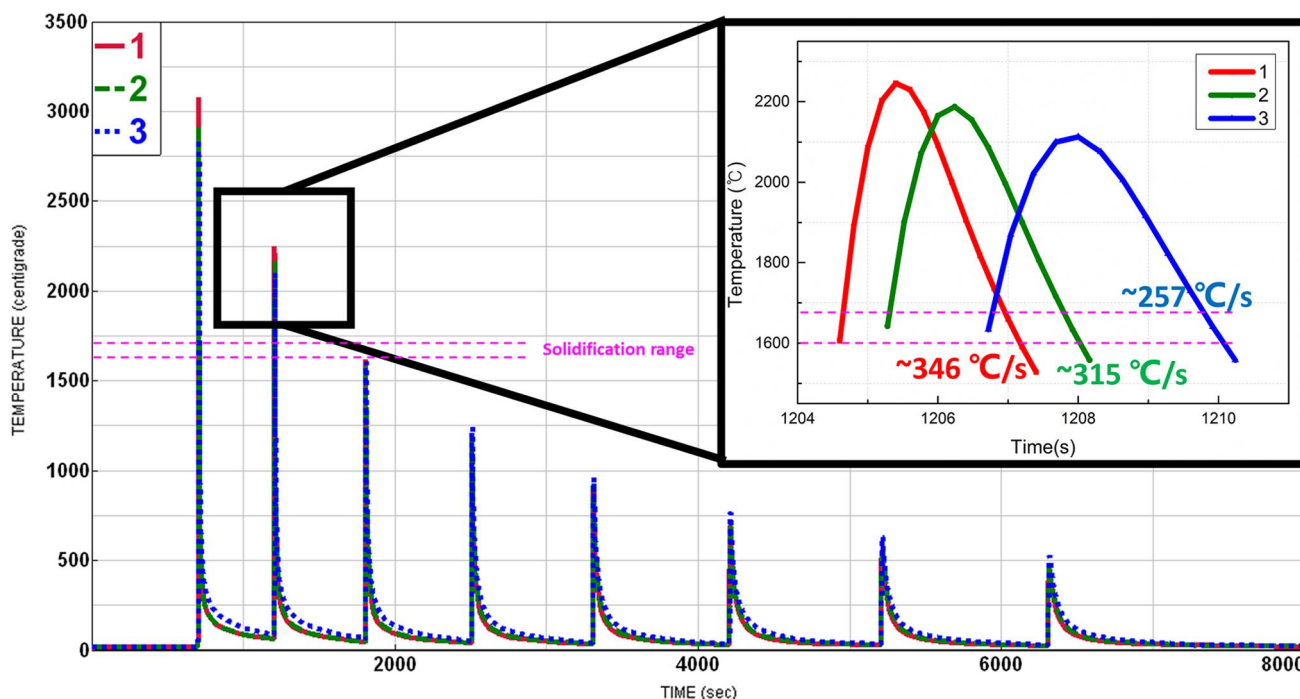


Fig. 6 Simulation of cooling rates in specimens F, M and S

tion, a greater number of equiaxed prior- β grains (specimen F) show weakened anisotropic properties than with mixture grains (specimens M and S).

- (2) Different welding speeds lead to a different weld pool shape, like its width and length. A higher welding speed contributes to a small temperature gradient (G) and a higher solidification rate (R) in all directions. Therefore, the optimal parameters required to form more equiaxed prior- β grains are those of specimen 1, as calculated to present a lower temperature gradient (G) and higher solidification rate (R).

Acknowledgements This work was supported in part by the Ministry of Science, ICT, and Future Planning of Korea through the National Research Foundation of Korea (NRF) Future Material Discovery Project of (NRF-2016M3D1A1023534) and by the Ministry of Trade, Industry and Energy (MOTIE, Korea) through the Technology Innovation Program (20004932).

References

- Rodrigues T A, Duarte V, Miranda R M, Santos T G, and Oliveira J P, *Materials* **12** (2019) 1121.
- Wu B, *J Manuf Process* **35** (2018) 127.
- Jeon S -H, Kim T -W, Lee Y -W, and Kim Y -C, *J Weld Join* **39** (2021) 632.
- Yi H -J, Kim J -W, Kim Y -L, and Shin S, *Korean J Mater Res* **31** (2021) 245.
- Graf M, Pradjadhiana K P, Hälsig A, Manurung Y H P, and Awiszus B, *AIP Conf Proc* **1960** (2018) 140010-1.
- Huda N, Kim J W, Ji C, Nam D -G, and Park Y -D, *J Weld Join* **39** (2021) 81.
- Dinovitzer M, Chen X, Laliberte J, Huang X, and Frei H, *Addit Manuf* **26** (2019) 138.
- Yi H -J, Kim J -W, Kim Y -L, and Shin S, *Met Mater Int* **26** (2020) 1235.
- Cheepu M, Lee C I, and Cho S M, *Trans Indian Inst Met* **73** (2020) 1475.
- Park J H, Cheepu M, and Cho S M, *Metals* **10** (2020) 365.
- Jun J H, Park J H, Cheepu M, and Cho S M, *Sci Technol Weld Join* **25** (2020) 106.
- Kik T, Moravec J, and Svec M, *Materials* **13** (2020) 5289.
- Kong Y S, Cheepu M, and Park Y W, *Trans Indian Inst Met* **73** (2020) 1433.
- Carroll B E, Palmer T A, and Beese A M, *Acta Mater* **87** (2015) 309.
- Ou W, Knapp G L, Mukherjee T, Wei Y, and DebRoy T, *Int J Heat Mass Transf* **167** (2021) 120835.
- Pradeep G V, Duraiselvam M, and Sivaprasad K, *J Mater Eng Perform* **31** (2022) 1009.
- Li Z, Liu C, Xu T, Ji L, Wang D, Lu J, and Fan H, *Mater Sci Eng A* **742** (2019) 287.
- Cheepu M, and Susila P, *Trans Indian Inst Met* **73** (2020) 1509.
- Xian G, Lee J, Cho S M, Yeom J T, Choi Y, and Kang N, *Weld World* **66** (2022) 847.
- Martina F, Colegrove P A, Williams S W and Meyer J, *Metall Mater Trans A* **46** (2015) 6103.
- Sokkalingam R, Sivaprasad K, Singh N, Muthupandi V, Ma P, Jia Y D, and Prashanth K G, *Prog Addit Manuf* (2022). <https://doi.org/https://doi.org/10.1007/s40964-022-00301-x>
- Kou S, *Welding Metallurgy*, John Wiley & Sons (2003).

Publisher's Note Springer Nature remains neutral with regard to jurisdictional claims in published maps and institutional affiliations.